Highlighting non-covalent interactions to molecular structure, electronic and vibrational spectra in a new hybrid organic-inorganic cobalt complex: synthesis, experimental and computational study

Meriam Tahenti, Noureddine Issaoui, Thierry Roisnel, Aleksandr S. Kazachenko, Maximiliano A. Iramain, Silvia Antonia Brandán, Omar Al-Dossary, Anna S Kazachenko, Houda Marouani

Highlighting non-covalent interactions to molecular Structure, Electronic and vibrational spectra in a new hybrid organic-inorganic cobalt complex: Synthesis, experimental and computational study

Meriam Tahenti[1], Noureddine Issaoui[2], Thierry Roisnel[3], Aleksandr S. Kazachenko[4,5], Maximiliano A. Iramain[6], Silvia Antonia Brandan[6], Omar Al-Dossary[7], Anna S. Kazachenko[4],Houda Marouani[1,*]

[1] University of Carthage, Faculty of Sciences of Bizerte, LR13ES08 Material Chemistry Laboratory, 7021, Bizerte, Tunisia.
[2] University of Monastir, Laboratory of Quantum and Statistical Physics, LR18ES18, Faculty of Sciences, Monastir 5079, Tunisia.
[3] Univ. Rennes, CNRS, ISCR (Institut des Sciences Chimiques de Rennes) – UMR 6226, F-35000 Rennes, France
[4] Siberian Federal University, pr. Svobodny 79, Krasnoyarsk, 660041 Russia.
[5] Institute of Chemistry and Chemical Technology, Krasnoyarsk Scientific Center, Siberian Branch, Russian Academy of Sciences, Akademgorodok, 50, bld.24, Krasnoyarsk, 660036 Russia.
[6] Cátedra de Química General, Instituto de QuímicaInorgánica, Facultad de Bioquímica, Química y Farmacia, Universidad Nacional de Tucumán, Ayacucho 471, (4000), San Miguel de Tucumán, Tucumán, Argentina.
[7] Departement of Physics and Astronomy, College of Science, King Saud University, BO Box 2455, Riyadh 11451, Saudi Arabia.
* Correspondence e-mail : issaoui_noureddine@yahoo.fr

Abstract: In this study, a novel hybrid organic-inorganic compound, 4-(ammoniummethyl)pyridinium tetracholoraobaltate(II) monohydrate, with non-centrosymmetric properties have been synthesized and characterized by several techniques of powder and single-crystal X-Ray diffraction, infrared IR and UV-Visible spectroscopies, and calorimetric (DSC) and the thermogravimetric (TG) analysis. The crystallization of this hybrid compound was found in a monoclinic system with a $P2_1$ space group. Additionally, the optimized structures of cation, anion and compound by using hybrid B3LYP method with 6-311++G(d,p) and 6-31+G(d) basis sets shown good correlations with the experimental data and the complete vibrational assignments and force constants are reported for three species. The surface morphology and the micrographs were checked by the scanning electron microscopy (SEM). The UV-Visible absorption spectrum has been used to study the optical properties and the energy gap of our compound.Hirshfeld surface (HS) analysis associated matched up with 2D fingerprint plots were used to confirm the existence of intermolecular and non-covalent interactions in the compound and confirmed by several topological approaches: Quantum Theory of Atom-in-Molecules (QTAIM), reduced density gradient (RDG) and molecular electrostatic potential surface (MEP). The frontier molecular orbitals HOMO and LUMO have been investigated for chemical reactivity and kinetic stability.

Keywords: X-Ray diffraction; molecular structure; IR spectra; Non covalent interactions; Hirshfeld Surface; DFT calculations.

1. Introduction

Pyridine and its derivatives possessed a significant role in heterocyclic chemistry [1-3]. The aromatic heterocyclic molecules associated to the hybrid materials are widely inquired in chemical [**4**], biological, and physics [**5**] research areas, as well as their application in various fields involving catalytic, magnetic, electrical conductivity, biochemistry, photochemistry and Non-Linear Optical (NLO) [**6**]. For the latest, the structure must present the characteristic of non-centrosymmetric materials. Telecommunications, information storage, optical computing, optical switching laser fusion reaction, medical diagnostics and signal processing where predicted in the application areas development of materials with outstanding nonlinear optical (NLO) responses. Pyridine-based ligands have reached a huge role over the last few decades due to their wide ability to produce compounds with several metals in different oxidation states [**7**]. According to the relative position of the amino group with respect to the pyridine group, (Aminomethyl)pyridines belong to the class of ligands which can act the role of a bridging and chelating ligand, although 4-(aminomethyl)pyridine (4AMP) type ligands can act as both a chelating agent or a bridging ligand. Consequently, they had attracted significant attention as biological activities such as antimicrobial [**8**], anti-inflammatory [**9**] and antiviral activity [**10**]. Special attention and interest in chemistry area evoke hybrid

compounds based on transition metal cobalt(II) halide because of its interesting properties not only its chemical properties but also their physical and biological nature which can be designed by several tools offered by molecular chemistry. Therefore, hybrid compounds containing $[CoX_4]^{2-}$ tetrahedral anions (X = halogen: Cl, Br) have a great interest across a wide fields of molecular materials and several interesting structural phase transitions [**11**, **12**]. $[CoCl_4]^{2-}$ anions own a good stabilizing behavior of the crystal structure. Their interactions with organic cations capable of creation of N-H···Cl and C-H···Cl hydrogen bonding have been widely reported an attention in literature [**13**, **14**]. The purpose of this research has been focused on experimental tools combined with theoretical calculations by using TD-DFT approach, gives more details information helped understand and delineate the characteristics and the proprieties of the title crystal. In this study, it was aimed to synthesize a novel hybrid material, $(C_6H_{10}N_2)[CoCl_4].H_2O$, and examine by single crystal and powder XRD studies in order to establish molecular geometry, crystallographic structure and atomic parameters. Intra and intermolecular interactions of crystal structure are performed by HS, AIM and RDG topological analysis. Besides, infrared spectroscopy allows identifying as precisely as possible the different functional groups and their vibrational assignments present in the compound. Hence, the optimized structures of cation, anion and compound by using hybrid B3LYP method with 6-311++G(d,p) and 6-31+G(d) basis sets agree with the experimental data which were used together with the scaled quantum mechanical force field (SQMFF) approach to perform their complete vibrational assignments [**15-17**]. To predict the reactivity of molecules, frontier molecular orbital HOMO-LUMO theory is employed and confirmed by the UV-Vis analysis. Thermal survey (DSC-TG) have been undertaken and discussed.

2. Results and Discussion

2.1. X-Ray Powder Diffraction Analysis

Fig.1a exhibits the experimental and simulated PXRD patterns. It is notice that the simulated X-ray powder diffraction pattern in a good agreement at the majority of the peak positions with the experimental one. We can assume that the elaborated crystals are pure and that the crystallographic data are correct.

After heating, the compound retains its crystallinity. XRD models for high temperature measurements show such behavior (Fig. 1b). The appearance and disappearance of the peaks after heating confirm that the crystallinity of our compound is preserved. On the other hand, our compound changes peaks with temperature to give a new phase at 150 °C, it corresponds to a dehydration of $(C_6H_{10}N_2)[CoCl_4].H_2O$. The anhydrous compound remains stable after cooling to room temperature.

(a) (b)

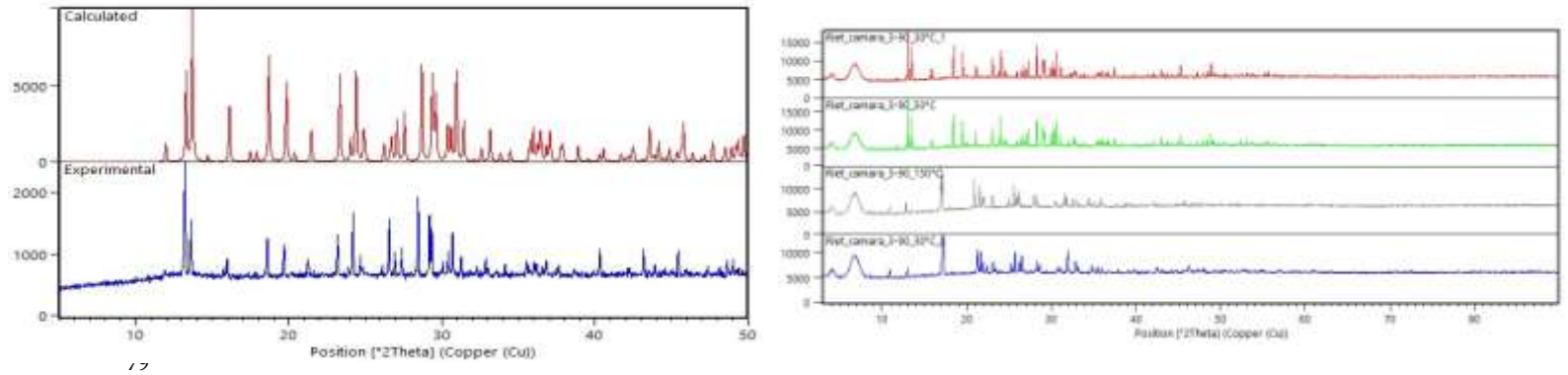

Figure 1. XRDP patterns simulated and experimental of $(C_6H_{10}N_2)[CoCl_4].H_2O$ (a). Thermal evolution of XRPD patterns during heating of the powder compound $(C_6H_{10}N_2)[CoCl_4].H_2O$ at 30, 50, 150 °C and cooling to room temperature (b).

2.2. SEM Morphologies

Scanning Electron Microscopy (SEM) shows the smooth and uniform particle morphology of the grown crystal $(C_6H_{10}N_2)[CoCl_4].H_2O$, in a wide size range 50 µm, 10 µm, 5 µm and 2 µm, given in micrometers, is exhibited in Fig.2. The surface morphology appears as an assemblage of uniformly fragments with a surface flat and evenly distributed, indicating good quality.

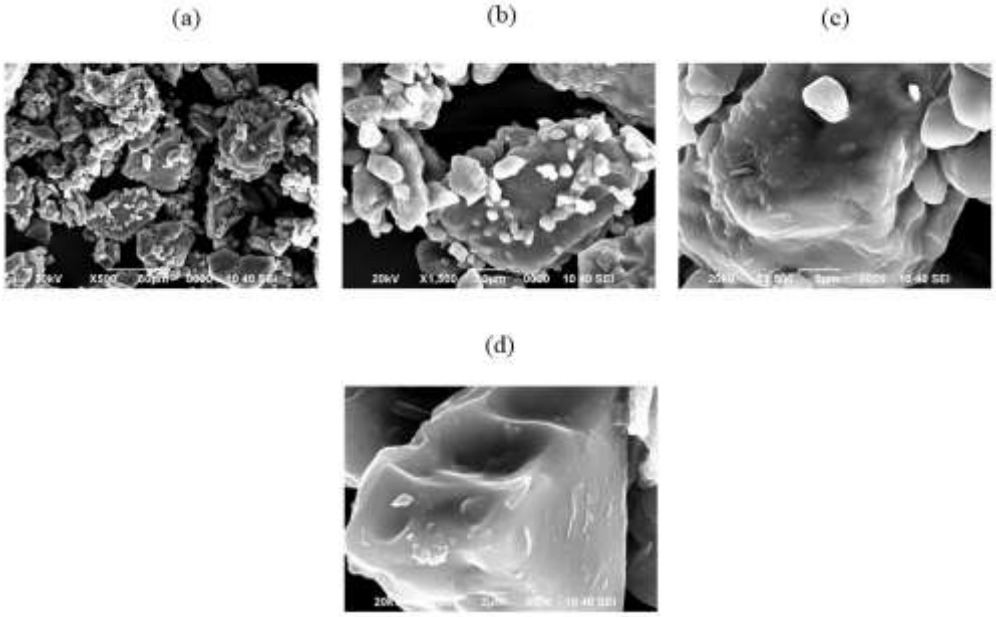

Figure 2. SEM images of $(C_6H_{10}N_2)[CoCl_4].H_2O$ at 50 µm (a), 10 µm (b), 5 µm (c) and 2 µm (d).

2.3. Single crystal X-Ray Diffraction

The single crystal X–ray analysis of non-centrosymmetric compound $(C_6H_{10}N_2)[CoCl_4].H_2O$ was carried out to study the crystal structure. The asymmetric unit contains both the cationic and anionic parts of complex, a $[CoCl_4]^{2-}$ anion of slightly distorted tetrahedral coordination, an organic dication $(C_6H_8N_2)^{2+}$ and a water molecule, where all the atoms occupy general positions (Fig. 3a). Fig. 3b predicted the optimized molecular structure of $(C_6H_{10}N_2)[CoCl_4].H_2O$ compound. Crystallographic data and details on the structure determinations of the title crystal at room temperature are given in Table 1 while Table 2 identifies a slight difference among chosen calculated geometrical parameters and empirical X-ray crystallographic parameters.

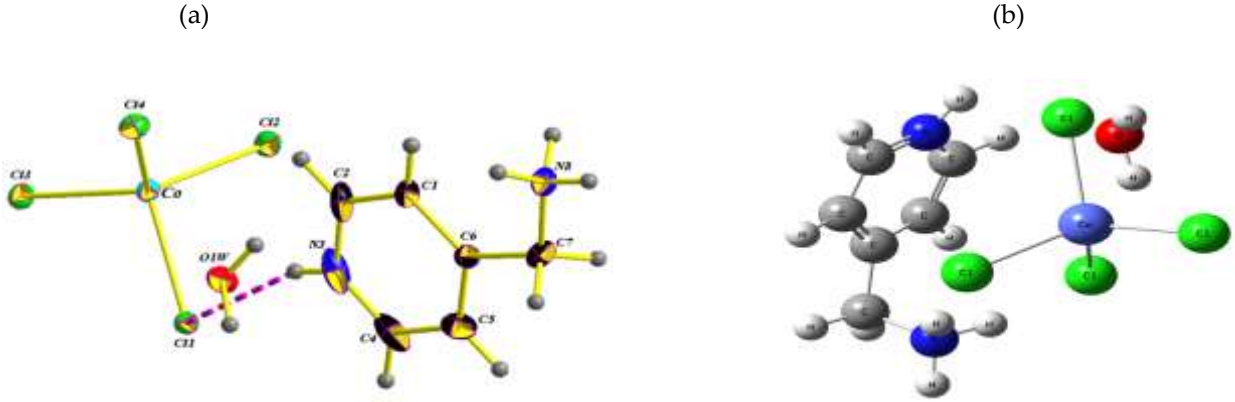

Figure 3. ORTEP representation of the asymmetric unit of $(C_6H_{10}N_2)[CoCl_4].H_2O$ with atom-labeling scheme. Displacement ellipsoids are drawn at the 50% probability level. Hydrogen bonds are denoted as dashed lines (a) and the optimized molecular structure (b).

120 **Table 1.** Crystallographic parameters details for $(C_6H_{10}N_2)[CoCl_4].H_2O$.

CCDC Number	**2,183,425**
Temperature	150 K
Empirical formula	$C_6H_{10}N_2{\cdot}CoCl_4{\cdot}H_2O$
Formula weight (g mol^{-1})	536.72
Crystal system	monoclinic
Space group	$P2_1$
a(Å)	6.1072 (9)
b(Å)	13.344 (2)
c(Å)	7.4940 (11)
β(°)	98.951(6)
Z	2
V($Å^3$)	603.28 (15)
F (000)	330
Mo Kα (mm^{-1})	μ= 2.28
Reflections collected	3902
Independent reflections	2183
Reflections with I > 2σ(I)	2127
R_{int}	0.030
Absorption correction:	*multi-scan* T_{min}= 0.529, T_{max} = 0.727
Refined parameters	145
R[F^2> 2⊚ (F)]	0.025
wR(F^2)	0.061
Goodness-of-fit on F^2	1.06
Flack parameter	−0.020 (16)

121

122 **Table 2.** Optimized and experimental bond lengths and bond angles (Å ,°) parameters of $(C_6H_{10}N_2)[CoCl_4].H_2O$.

Bond length (Å)	***X-ray***	***Calculated***
Inorganic		
Co—Cl1	2.3813 (9)	2.4231
Co—Cl2	2.2663 (10)	2.4275
Co—Cl3	2.2547 (11)	2.2500
Co—Cl4	2.2741 (11)	2.5342
Cl1—Cl2	3.5976 (13)	3.9957
Cl1—Cl3	3.6665 (14)	3.66536
Cl2—Cl4	3.7323 (14)	3.70403
Cl3—Cl4	3.7963(15)	3.89951
Organic		
N3—C2	1.348 (6)	1.3614
N3—C4	1.341 (7)	1.3599
N8—C7	1.469 (5)	1.5272
C4—C5	1.376 (7)	1.3985
C5—C6	1.395 (5)	1.4073
C6—C7	1.497 (6)	1.5183
Bond angles (°)	***X-ray***	***Calculated***
Inorganic		
Cl1—Co—Cl2	103.39 (4)	110.9214

Cl1—Co—Cl3	106.60 (4)	103.2575
Cl1—Co—Cl4	106.19 (4)	114.0167
Cl2—Co—Cl3	115.12 (4)	123.4439
Cl2—Co—Cl4	110.58 (4)	96.5559
Cl3—Co—Cl4	113.92 (4)	109.0466
Organic		
N3—C2—C1	110.08 (16)	119.3761
C4—N3—C2	122.8 (4)	123.2771
N3—C4—C5	119.2 (4)	118.6842
N8—C7—C6	109.98 (16)	107.6369
C2—C1—C6	110.16 (18)	119.1596
C4—C5—C6	111.33 (17)	119.6935
C1—C6—C5	111.4 (2)	119.1267
C1—C6—C7	111.79 (18)	120.1642
C5—C6—C7	111.2 (2)	119.7107

Notably, the 4-(ammonium methyl)pyridinium (4AMP), $(C_6H_8N_2)^{2+}$, is described by C-C bond lengths observed around 1.419 Å and calculated toward 1.441 Å, an average value of the bond angles equal to 111.37°, this last value is noted for the angle (C4-C5-C6), comparable to the theoretical values 119.57°. Indeed the C-N calculated distance varies from 1.3599 to 1.5272 Å, and observed by XRD from 1.341 (7) to 1.469 (5) Å, this is explained by the protonation of the organic cation. The geometric parameters of the organic part do not present any peculiarity to those encountered in other similar compounds [**18, 19**]. On the other hand, the geometric of $[CoCl_4]^{2-}$ group was tetrahedral with a cobalt atom that is surrounded by four chloride anions. The calculated length of the Co-Cl bond varies from 2.2500 up to 2.5342 Å, then the experimental varies from 2.2547 (11) up to 2.3813 (9) Å. The average value of the bond angles Cl-Co-Cl observed by XRD is 109.3° and the calculated is 109.5°. These geometries are comparable to other halogenocobaltates reported in the literature [**13, 20**]. As expected, the four-coordinate cobalt (II) geometry index of $[CoCl_4]^{2-}$ defined by Alvarez by:

$$\boldsymbol{\tau_4} = \frac{\mathbf{360-(\alpha+\beta)}}{\mathbf{141}} = \frac{\mathbf{360-(115.12+113.92)}}{\mathbf{141}} = 0.928$$

Where, $\boldsymbol{\alpha}$ and $\boldsymbol{\beta}$ correspond to the largest angles in the four coordinate species. As a consequence, we can admit that the compound gives a $\boldsymbol{\tau_4}$ close to 1 indicating a slightly deformed tetrahedral geometry [**14**]. It's clearly shown that the projection of the unit-cell content along the $\vec{\boldsymbol{a}}$ axis, can be described by anionic chains which develop onto *bc*plane, formed by tetrachlorocobaltate anions and water molecules connected together through hydrogen bonds O-H···Cl. These chains spread out parallel to the $(01\bar{\mathbf{1}})$ planes to form inorganic layers between which the 4AMP are ensured via hydrogen bonds N-H···O, N-H···Cl, O-H···Cl and C-H···Cl, thus forming a three-dimensional network (Fig. 4a-4b).

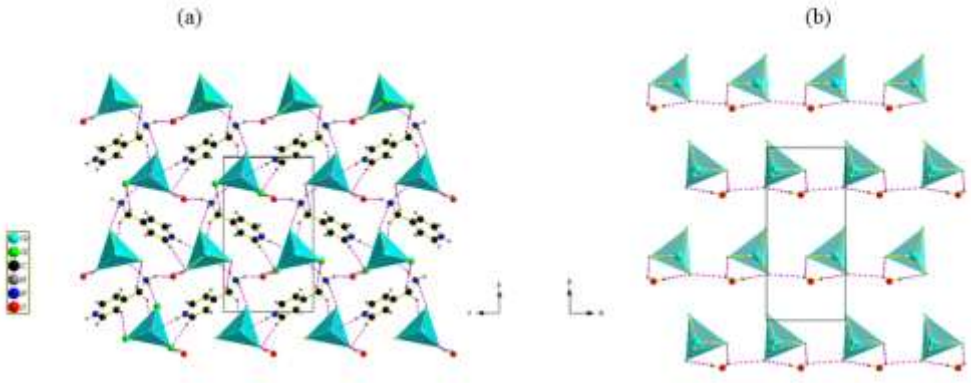

Figure 4. Packing of the title compound viewed along *bc* plane (a) and a view along *ab*plane of the inorganic part and the patterns of hydrogen bonding (b) in $(C_6H_{10}N_2)[CoCl_4].H_2O$.

In this monoclinic unit, the different entities are linked to each other via 3 types of hydrogen bonds presented Table 3. The donor-acceptor distances $d_{N\text{-}H\cdots Cl}$ are ranging from 3.198(3) Å to 3.718(3) Å, give appearance to $\boldsymbol{R_2^1}(4)$ and $\boldsymbol{R_4^6}(14)$ (Fig. 5a) [**21**]. Whereas, $d_{C\text{-}H\cdots Cl}$present an average of 3.683 Å gives birth to graphs $\boldsymbol{R_2^2}(7)$ (Fig. 5b).

Three bonds O-H···Cl which ensure the bond between the water molecules and the chloride ions of the inorganic group $[CoCl_4]^{2-}$ forming infinite chains of $(\boldsymbol{ClH_2O})_n^{n-}$, whose distances vary between 2.47 (2) Å – 2.79 (3) Å, giving rise to chains of $\boldsymbol{C_2^1}(\mathbf{4})$which are along the axis $\vec{\boldsymbol{a}}$ in z=1/4 and 3/4 (Fig. 5c). The N-H···O type bonds linking the nitrogen protons to the oxygen atoms of the water molecules whose $d_{N\text{-}H\cdots O}$=2.686 (5) Å [**22**]. According to Brown's theorem, this bond is considered a strong bond [**23**].

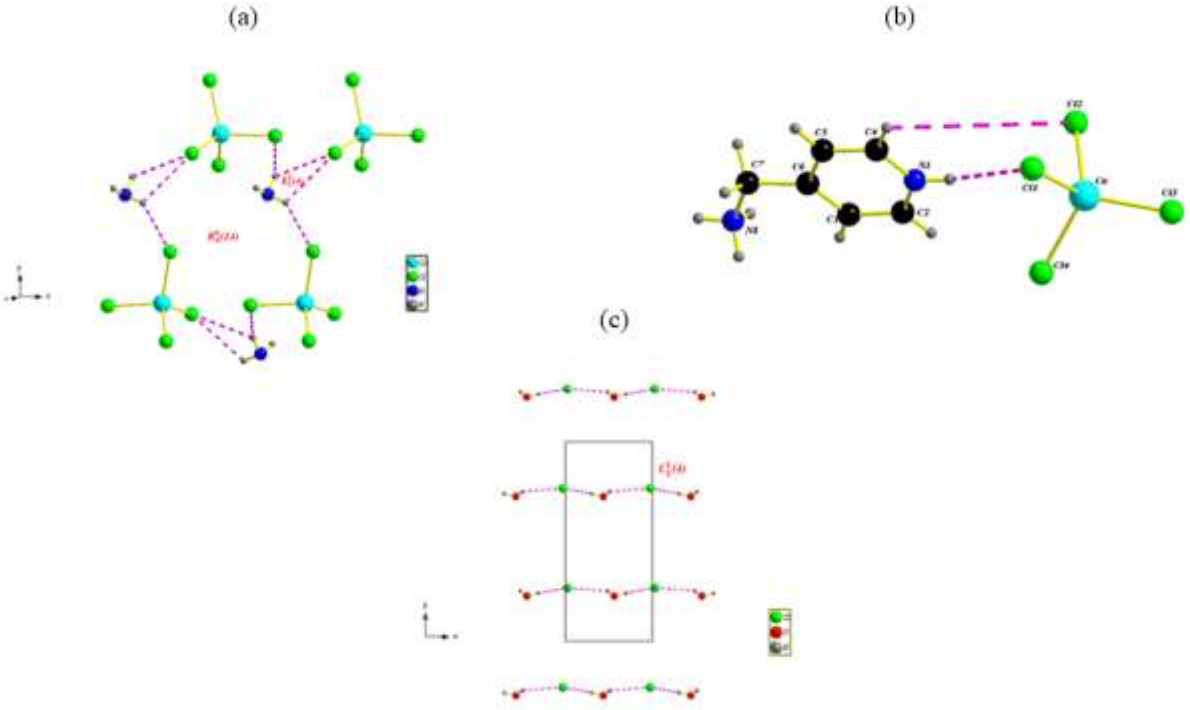

Figure 5. Different types of Hydrogen bond motifs in $(C_6H_{10}N_2)[CoCl_4].H_2O$. The dotted lines indicate the hydrogen bonds.

Table 3. H-bonds geometry of $(C_6H_{10}N_2)[CoCl_4].H_2O$.

D—*H*···*A*	*D*—H (Å)	H···*A*(Å)	*D*···*A* (Å)	*D*—H···*A*(°)
N3—H3···Cl1	0.86 (2)	2.41 (3)	3.230 (4)	160 (5)
N8—H8A…Cl4^{iii}	0.90 (2)	2.46 (3)	3.242 (4)	146 (4)
N8—H8B…O1W^{iii}	0.87 (2)	1.89 (3)	2.686 (5)	151 (4)
N8—H8C···Cl1^{ii}	0.88 (2)	2.53 (3)	3.319 (4)	151 (4)
N8—H8C···Cl3^{iv}	0.88 (2)	2.80 (4)	3.274 (4)	115 (3)
O1W—HW1A···Cl1^{ii}	0.85 (1)	2.55 (3)	3.276 (3)	145 (3)
O1W—HW1A···Cl2^{iv}	0.85 (1)	2.79 (3)	3.321 (3)	122 (3)
O1W—HW1B···Cl2^{ii}	0.84 (1)	2.47 (2)	3.242 (3)	153 (4)
C4—H4···Cl2^{i}	0.95	2.69	3.621 (5)	167
C7—H7A···Cl3^{ii}	0.99	2.72	3.548 (4)	146
C7—H7B···Cl1^{iii}	0.99	2.81	3.624 (4)	140

Symmetry codes :*(i) x−1, y, z; (ii) −x+1, y+1/2, −z+1; (iii) x, y, z+1; (iv) −x+2, y+1/2,*

As in the published article [24], B3LYP/6-311++G** calculations were performed to investigate structural, electronic, topological and vibrational studies. In the Co, Cr, Cu transitions metal that method can be used.In that published article, the (CrO_4^{2-}) anions are connected to the 2-phenylethylammonium cations through N-H…O and C-H…O

hydrogen bonds, forming a two-dimensional arrangement. In the structure of this compound, the $[CoCl_4]^{2-}$ anion has slightly distorted tetrahedral coordination linked to an organic dication $(C_6H_8N_2)^{2+}$ with a water molecule connected together through hydrogen bonds O-H···Cl. Here, hydrogen bonds N-H···O, N-H···Cl, O-H···Cl and C-H···Cl forming a three-dimensional network.

2.4. *HS analysis*

In the field of crystal engineering, the analysis of the surface of molecular system and the intermolecular interactions was studied to perform and to compare the molecular contributions of various intermolecular contacts around the packing of crystal to create the crystal structure trough the Crystal Explorer 3.1 program. Single-crystal X-ray diffraction is absolutely sufficient to determine the exact structure of this material, Hirshfeld surface analysis is a quantitative study that calculates the percentage of each interaction that exists in this compound, and it can be a complementary study to XRD which is a qualitative study.

In order to represent the shape details and the molecular packing in the crystal, Fig. 6 shows the HS mapping over the asymmetric unit (a), the d_{norm} (-0.480 - 1.090) map (b) of $(C_6H_{10}N_2)[CoCl_4].H_2O$. This latter is represented in 4 bright red spots matches to the strong N-H···Cl, C-H···Cl and O-H···Cl interactions as well as the other visible spots (blue and white) due to the H···H and C···C contacts.

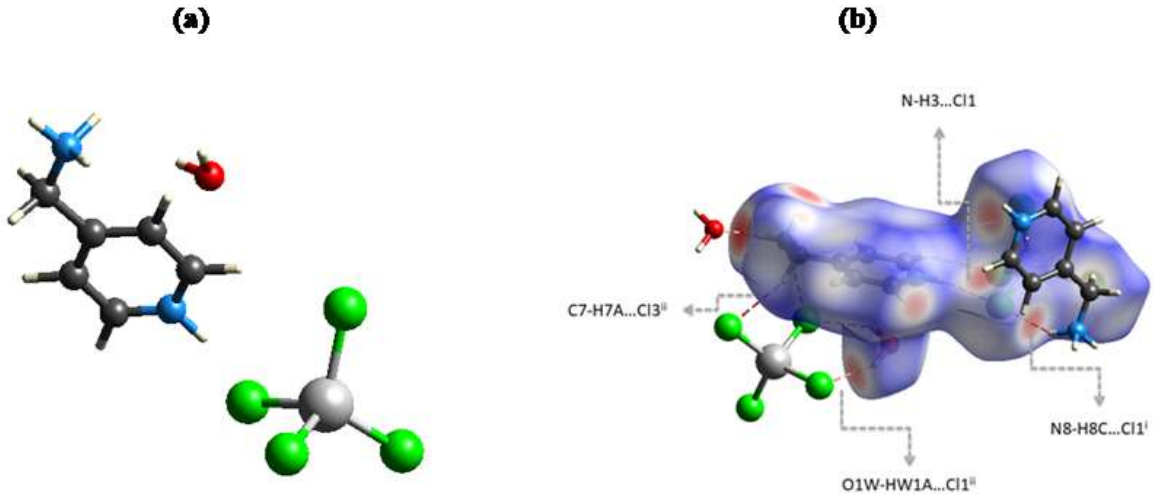

Figure 6. The asymmetric unit (a), Hirshfeld surfaces mapped with d_{norm}(-0,480 - 1,090) (dotted lines "red" represent hydrogen bonds) (b) of $(C_6H_{10}N_2)[CoCl_4].H_2O$.

As displayed in Fig. 7a and Fig. 7b, the 2D fingerprint plots and the different percentages of intermolecular contacts, respectively, are the signs of the intermolecular interactions present in the structure of the studied compound $(C_6H_{10}N_2)[CoCl_4].H_2O$. As it is expected in 2D fingerprints, H···Cl/Cl···H intermolecular contacts occupy most of the HS (63.5%) and appear as two symmetrical wings with a large long peak of sum ($d_e + d_i$ = 2.4 Å) smaller than the sum of the van der Waals radii of the hydrogen (1.09 Å) and chlorine (1.75 Å) atoms. As well as, the value of enrichment ratio ER_{HCl} equal to 1.60 are developed in the crystal structure with the creation of N-H···Cl, C-H···Cl and O-H···Cl H-bonds. The next largest strong hydrogen bond interaction portion of 18.3% was contributed to H…H interactions with $d_e + d_i$ = 1.8 Å. Table 4 shows that these contacts adopt an ER_{HH} value equal to 0.62 far from unity, $(C_6H_{10}N_2)[CoCl_4].H_2O$ has several hydrogen atoms (S_H = 54.45%), therefore H···H interactions are preferential (Fig. 7b). Also it is seen from Hirshfeld surface area that O···H/H···O intercontacts occupy 5.6% and appear as two sharp spikes pointing down with $d_e + d_i$ = 1.8 Å with a high value of ER_{OH} = 1.81 allow to stabilize the interactions in crystalline packaging with the formation of hydrogen bonds of the N-H···O type which are strong hydrogen bonds d(O-H) = 2.686 (5)Å. On the other hand, 2.5% of HS is attributed to the C···H/H···C contacts which appear with $d_e + d_i$ = 2.3 Å. The rest of the intermolecular contacts N···Cl/Cl···N, Co···Cl/Cl···Co, Cl···Cl, C···Co/Co···C, H···Co/Co···H, N···H/H···N et Cl···O/O···Cl are found to be less than 2%, which causes a low value of ER. The small segments delimited by a blue outline observed on the Curvedness map, the absence of red and blue triangles on the Shape index

map as shown in Fig.7c and the null contribution of the C···C contacts on the HS, reveal the absence of π-π interactions in our crystal packing [**25**]. This confirms the results observed by X-ray diffraction.

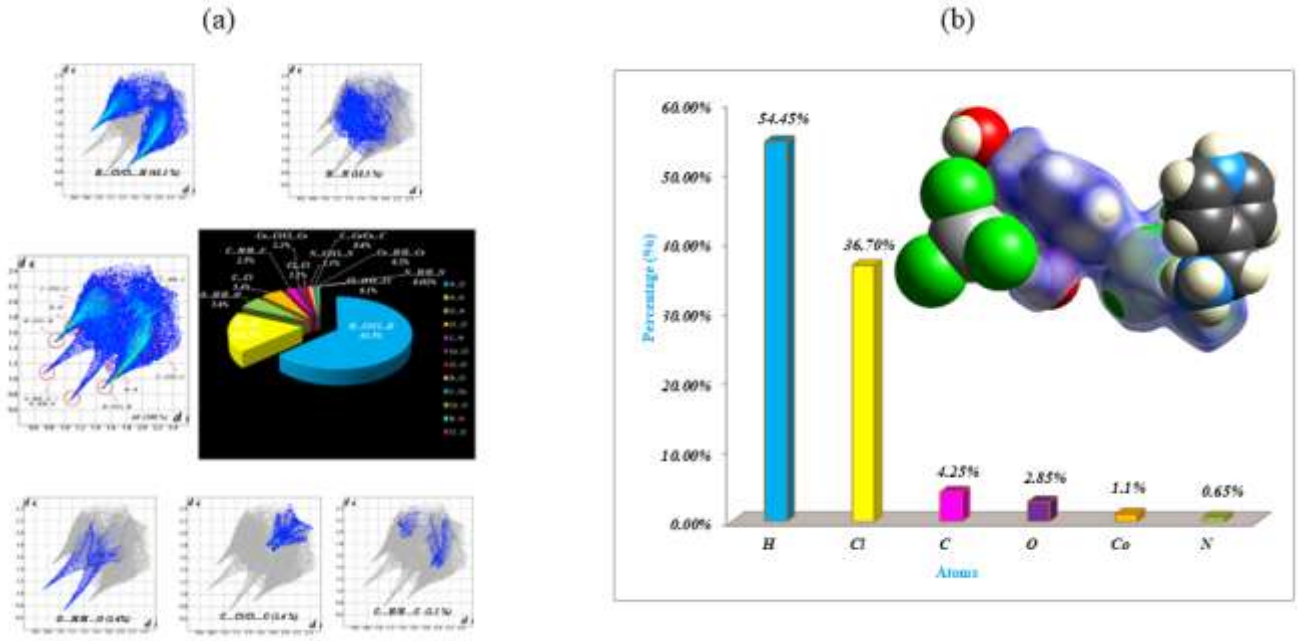

Figure 7.2D fingerprint plots of major interactions in crystal stacking (a), Atom's Percentage (b) of $(C_6H_{10}N_2)[CoCl_4].H_2O$.

Table 4. Enrichment ratio (ER) of $(C_6H_{10}N_2)[CoCl_4].H_2O$.

ER	H	C	Co	Cl	N	O
H	0.62	0.54	0.42	1.60	0.29	1.81
C		-	-	1.74	-	-
Co			-	1.38	-	-
Cl				0.08	2.34	0.05
N					-	-
O						-
%surface	**54.45**	**4.25**	**1.1**	**36.7**	**0.65**	**2.85**

2.5. *FTIR Spectroscopy*

B3LYP/6-311++G(d,p) calculations have optimized the structure of anion with D_{2d} symmetry while the corresponding to cation and compound with C_1 symmetries. The structure of compound was optimized with the B3LYP/6-31+G(d) level of theory because imaginaries frequencies were obtained with the 6-311++G** basis set. The 9 normal modes of vibration expected for the $[CoCl_4]^{2-}$ anion are classified as $2A_1 + B_1 + 2B_2 + 2E$, being the 2 B_2 and 2 E modes active in infrared and all modes active in Raman. From harmonic force fields for each species computed with the SQMEF procedure and considering PED (Potential energy distribution) ≥7-10% the complete vibrational assignments were performed taking into account the normal internal coordinates, scaling transferable factors and the Molvib program [**15-17**]. Fig. 8 shows the experimental and theoretical IR spectra of the title compound and its cation and anion. Fig. 9 shows the predicted Raman spectra for those three species by using the B3LYP/6-311++G(d,p) and B3LYP/6-31+G(d) methods. The IR absorption bands have been compared with other assigned to similar compounds [**26-29**]. Here, the vibrational assignments were performed using normal internal coordinates, transferable scaling factors and the harmonic force fields calculated with the SQMFF methodology and the Molvib program [**15-17**]. In Table 5 are summarized observed and calculated wavenumbers and assignments for the compound and its cation and anion in gas phase by using those different hybrid B3LYPMethods.The experimental IR bands in

The region high-wavenumbers at 3545 and3471 $cm^{-1}$are assigned to the symmetric and asymmetric stretching of O-H group [**30**]. Both bands indicates the presence of water molecule in $(C_6H_{10}N_2)[CoCl_4].H_2O$ [**31**]. Bands between 3471 and 2986 cm^{-1} are attributed to the stretching modes of NH_3^+ and CH_2 groups and, to C-H stretching vibrations of the aromatic ring predicted between 3443 and 3042 cm^{-1}. The broadening of bands between 2833 and 2613 cm^{-1} is due to hydrogen bonds interactions because the two N20-H22 and N20-H23 bonds of NH_3^+ group forming the N20-H22···Cl5 and N20-H23···Cl3 interactions. Hence, the symmetric NH_3^+ stretching modes predicted at 2648 $cm^{-1}$is assigned at 2833 cm^{-1}while the symmetric deformation of this group predict at 1663 cm^{-1} is assigned to the strong band at 1644 cm^{-1}. The effect of lowering the frequencies is observed in the shifting predicted for the N3-H11 bond from 3442 cm^{-1} in the cation to 2902 cm^{-1} in the compound. Additionally, the vibrations of (C=C), (C=N), (C-C), and (C-N) stretching modes are predicted at lower wavenumbers in the compound and, hence, they are assigned between 1644 up to 770 cm^{-1}. The bending modes of the aromatic ring (βN3-H11 and C-H) are assigned at different wavenumbers, as compared with the cation due to the presence of water and to the interactions of H bonds. Thus, the deformation modes of water and NH_3^+ groups are assigned between1644 and 1510 cm^{-1}, as predicted by calculations and as observed in Table 5. Due to the different H bonds, some librations modes of water are coupled, as was observed for the twisting mode [**32**]. Thus, the IR bands at 1610 and 672 cm^{-1} are assigned to deformation and wagging modes of water molecule while the rocking and twisting modes are predicted at 239 and 51 cm^{-1} but not assigned. Moreover, the vibration bands located among 1000 to 500 cm^{-1} were assigned to some out-of-plane C-H deformation modes, to CH_2 twisting modes, to C-C stretching and to vibrations of ring, as described in Table 5.

Observing the predicted wavenumbers for the anion by SQM calculations, it is easy to see that the presence of cation produce shifting in the positions of vibrations modes corresponding to compound toward lower wavenumbers. Note that all vibration modes related to anion could not be assigned because the IR spectrum was recorded up to 500 cm^{-1}. A very important resulted obtained from vibrational analyses are the strong couplings observed between the N20-H22-Cl5 and N20-H23-Cl3 deformation modes due to the H bonds interactions involved while the other interaction N10-H11···O24 only produces coupling of twisting mode of water molecule.

In general, the theoretical wavenumber agrees well with those obtained experimentally despite that the experimental IR spectrum is recorded in the solid state whereas the theoretical is performed for isolated molecules.

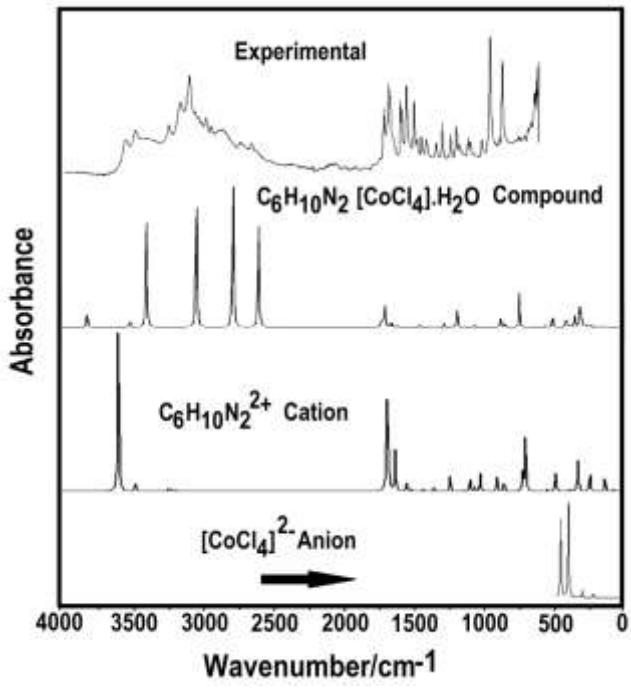

Figure 8. Experimental and calculated FTIR spectra of $(C_6H_{10}N_2)[CoCl_4].H_2O$ compound.

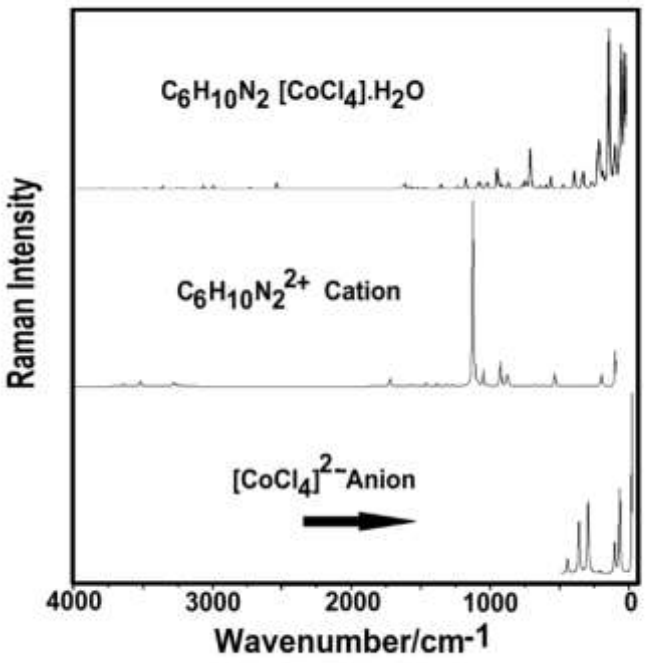

Figure 9. Predicted Raman spectra for hybrid compound and it cation and anion species by using the B3LYP/6-31+G(d) and B3LYP/6-311++G(d,p) methods.

Table 5. Observed and calculated wavenumbers (cm^{-1}) and assignments for $(C_6H_{10}N_2)[CoCl_4].H_2O$ and its cation and anion in gas phase by using hybrid B3LYP/6-311++G** Method.

Exp.[a]		$(C_6H_{10}N_2)^{2+}$ [a]	$[CoCl_4]^{2-}$ [a]		$(C_6H_{10}N_2)[CoCl_4].H_2O$ [a]	
IR	SQ	Assignments[a]	SQ	Assignments	SQ	Assignments[a]
3545					365	ν_aH_2O
3471	344	ν_aNH_3			336	ν_aNH_3
3471	344	νN3-H11			324	ν_sH_2O
3392s	343	ν_aNH_3			314	νC8-H9
3226	332	ν_sNH_3			312	νC12-H13
3143s	314	ν_aCH_2			311	νC6-H7
	309	νC2-H10				
3077s	309	νC4-H12			309	νC14-H15
	307	νC5-H13				
	307	νC1-H9				
2986	304	ν_sCH_2			301	ν_aCH_2
2951s					296	ν_sCH_2
2920					290	νN3-H11
2833					264	ν_sNH_3
2613					247	ν_aNH_3
1644s					166	δ_sNH_3
1644s	162	νC1-C2,νC4-C5			163	δ_aNH_3,δN20H22Cl5
1610s	158	δ_aNH_3			163	βN10-H11
1610s	158	δ_aNH_3			160	δH_2O
1610s	156	βN3-H11			158	δ_aNH_3
1610s					155	δN20H23Cl3,δ_aNH_3

1524s					152	νC6-C16,νC14-C16
1510s	148	νC6-C7,δCH_2			150	$\delta_a NH_3$,δN20H23Cl3
1476s	145	βC2-H10,βC4-H12			145	δCH_2, δN20C17C16
1419s	143	δCH_2			139	ρCH_2, ρNH_3
1399					137	βC6-H7, βC14-H15,νC6-C8
1366	137	βN3-H11,νC1-C2			133	βC8-H9, βC12-H13
1330	129	νC5-C6,νC1-C6			128	δN20H22Cl5,δN20H23Cl3
1258	128	νC6-C7			124	δN20H23Cl3,δN20H22Cl5
1211s	122	νC4-N3,νC2-N3			120	δN20H22Cl5,$\delta_a NH_3$
1211s					120	δN20H22Cl5,δN20H23Cl3
1148s					113	δN20H22Cl5,δN20H23Cl3
1148s	118	βC1-H9, βC5-H13			111	γC6-H7,δC12H13O24
1107s	108	νC4-N3,νC2-N3			111	δN20H23Cl3,δN20H22Cl5
1083	103	$\delta_s NH_3$			106	δN20H23Cl3,δN20H22Cl5
1017	102	βR_1			106	δN20H23Cl3,δN20H22Cl5
1007	982	νC2-N3,νC4-N3			997	βR_1νC8-N10,νC12-N10
993sh	972	γC2-H10,γC4-H12			963	γC14-H15,γC12-H13
930sh	966	γC4-H12,γC2-H10			954	νC17-N20
921m	934	wagCH_2			937	γC6-H7,γC8-H9
860vs	879	ρCH_2			852	δN20H22Cl5,δN20H23Cl3
860vs	829	γC2-H10,γC4-H12, γC1-H9,γC5-H13			837	δN20H22Cl5,δN20H23Cl3
	827	γC5-H13,γC1-H9				
792w	816	νC1-C6,νC5-C6			818	δN20H23Cl3,γC16-C17
770vs	686	τR_1			780	νC16-C17
770vs					714	τR_1,γC16-C17
672w	676	γN3-H11			678	wagH_2O
648w	648	βR_2			658	βR_2,βR_3
578w	564	τwCH_2			574	δN20H22Cl5, δN20C17C16
533m	523	βR_3			504	δN20H22Cl5,γC16-C17
510s	460	τR_2,γC6-C7			449	δN20H22Cl5,δN20H23Cl3
					425	δN20H22Cl5
	401	τR_2,τR_3	399	$\nu_a CoCl_2$	392	τR_2,τR_3
	359	βC6-C7	347	$\nu_a CoCl_2$	349	δN20H23Cl3
			341	$\nu_a CoCl_2$	346	δN20H23Cl3,$\nu_a CoCl_2$
	307	ρ'NH_3			329	δN20H22Cl5,δN20H23Cl3
	301	ρNH_3			285	νH22-Cl5
			255	w$agCoCl_2$	251	$\nu_a CoCl_2$,νH23-Cl3
					249	νH23-Cl3
			235	$\tau_w CoCl_2$	239	ρH_2O
	220	τR_3			219	δN20H22Cl5,$\nu_s CoCl_2$
					205	$\nu_a CoCl_2$,$\nu_s CoCl_2$
			182	δCl2Co1Cl4	184	δN20H23Cl3,δN20H22Cl5
			153	δCl3Co1Cl5	158	δN20H23Cl3,δN20H22Cl5
					139	δCl2Co1Cl3,δN20H22Cl5
					129	δN20H22Cl5,δN20H23Cl3
	113	νC7-N8			106	δCl2Co1Cl3,τwH23-Cl3
					99	τwH22-Cl5,τwH23-Cl3

				92	τwH22-Cl5,τC17-C16, wag$CoCl_2$
				83	τwH23-Cl3,δN20H23Cl3
				72	δN20H23Cl3,τwH23-Cl3
61	τC7-C6	62	ρ$CoCl_2$	62	δCl2Co1Cl3
58	δN8C7C6			51	τwH13-C12,τwH_2O
				47	τwH23-Cl,3ρ$CoCl_2$
				32	τwNH_3
26	τwNH_3			28	δCl5Co1Cl4

Abbreviations: ν, stretching; β, deformation in the plane; γ, deformation out of plane; wag, wagging; τ, torsion; ρ, rocking; τw, twisting; δ, deformation; a, antisymmetric; s, symmetric; [a]This work, [b]From scaled quantum mechanics force field with B3LYP/6-311++G** method, [c]From scaled quantum mechanics force field with B3LYP/6-31+G* method.

3.6. Force Constants

The scaled force constants are interesting parameters that predict the forces of different bonds and, also changes related to these factors allow justifying, for instance, formation of H bonds interactions. Here, these factors were calculated from harmonic force fields for the compound and its cation and anion using the B3LYP/6-31+G(d) and B3LYP/6-311++G(d,p) methods [**15-17**]. In Table 6 are shown comparisons of obtained values for those three species. Comparing first the force constants of cation and compound, we observed that *f(νN-H)*constants of cation undergoes a significant decreasing when the anion is incorporate to compound, in particular, the $f(\nu N\text{-}H)_{NH3}$ constant related to NH_3 group decrease from 6.44 to 4.23 mdyn $Å^{-1}$, as a consequence of two N-H···Cl interactions. A similar effect is observed in the deformation constant of this group. Comparing the constants of anion and compound the *f(νCo-Cl)* present a decreasing while the *f(δ(Cl-Co-Cl)* constant increases due to the two N-H···Cl interactions. On the other hand, the force constants related to the water molecule present similar values to reported for monohydrate trehalose (OH stretching, 7.49 mdyn $Å^{-1}$; while OH deformation, 0.795 mdyn Å rad^{-2}) [**32**] because the compound only a H bond interaction forms with the water molecule.

Table 6. Scaled internal force constants for $(C_6H_{10}N_2)[CoCl_4].H_2O$ and its cation and anion in gas phase by using hybrid B3LYP/6-311++G** and B3LYP/6-31+G* Methods.

	B3LYP Method[a]		
Force	6-311++G**		6-31+G*
constants	Cation[b]	Anion[c]	Compound
f(νO-H)			6.67
f(νN-H)	6.56		5.35
$f(\nu N\text{-}H)_{NH3}$	6.44		4.23
$f(\nu CH_2)$	5.27		4.93
f(νC-H)	5.21		5.33
f(νCo-Cl)		1.64	0.91
$f(\delta CH_2)$	1.00		1.16
$f(\delta NH_3)$	0.49		0.74
f(δ(Cl-Co-Cl)		1.28	3.28
$f(\delta H_2O)$			0.86

Units are mdyn $Å^{-1}$ for stretching and mdyn Å rad^{-2} for angle deformations,[a]This work.

3.7. Optical behavior

The solid-state UV–Vis spectrum between 200 and 800 nm excitation length of $(C_6H_{10}N_2)[CoCl_4].H_2O$ at room temperature, is displayed experimentally in Fig. 10a.

In the UV-visible region, the experimental spectrum exhibits three maximums absorption bands at 430, 470 and 559 nm. These obtained bands can be assigned to the d-d transitions of orbitals of the cobalt ions Co^{2+} according the literature [**33**], in its quadruplet coordinated tetrahedral symmetry placed in the center of the distorted tetrahedron formed by four Cl^- ions [**34**].

In the aim to study the reactivity and the kinetic stability of the molecule, Tauc's model is used to estimate the optical band gap (Eg) of $(C_6H_{10}N_2)[CoCl_4].H_2O$ (Fig. 10b), by using the equation:

$$(\alpha.h\nu)^2=(h\nu - Eg)$$

Where hυ was the incident's photon energy, h was the Plank's constant and υ was the incident's photons frequency [**35**]. This value was found to be Eg = 2.325 eV, reveals that our compound possessed a semiconductor characteristic. This value matched well to the value found by the LUMO-HOMO orbital theory $E_{HOMO/LUMO}$ = 2.35 eV.

The band gap value of $(C_6H_{10}N_2)[CoCl_4].H_2O$ is comparable to the calculated values of the gap energies found in other compounds containing $[CoX_4]$ (with X = Br and Cl) [**36**].

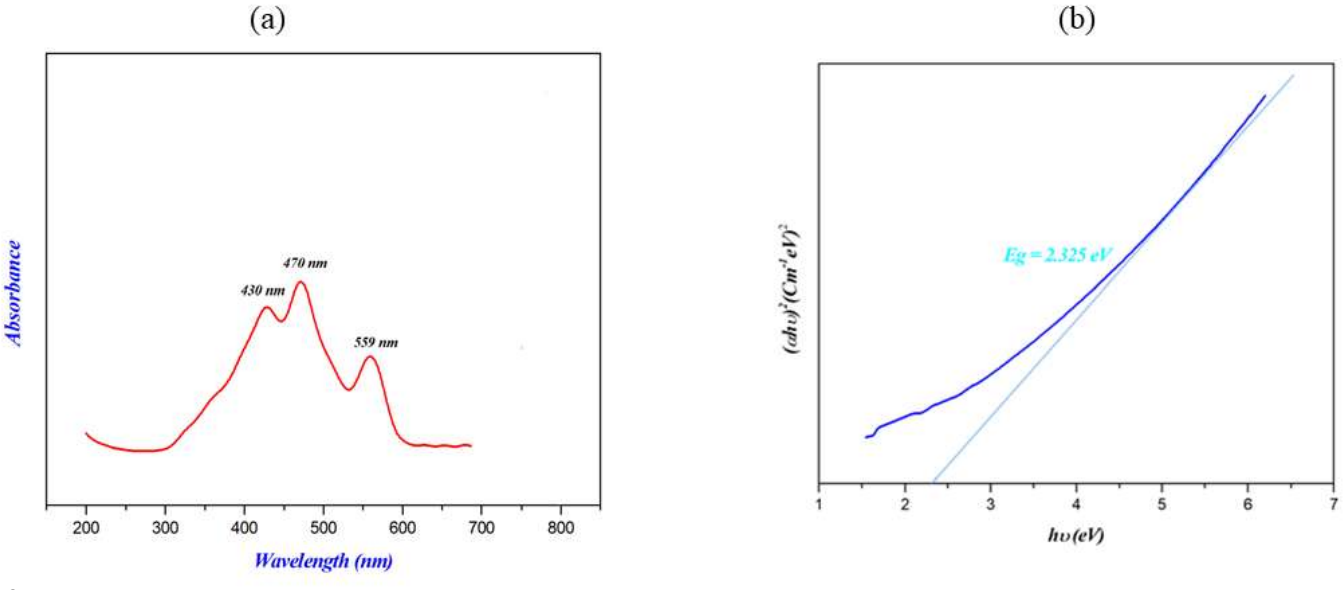

Figure 10. Solid-state UV-Vis spectrum (a) and determination of the energy gap obtained via the Tauc model of $(C_6H_{10}N_2)[CoCl_4].H_2O$ (b).

2.3. *Thermal Analysis*

The results of the calorimetric (DSC) and the thermogravimetric (TG) analysis for $(C_6H_{10}N_2)[CoCl_4].H_2O$ are depicted in Fig. 11. The endothermic peak appeared on the DSC curve at 375 K, is accompanied by weight loss equal to 3.32 % on the TG curve (calculated: 3.35%). This corresponds to the departure of the water molecule. The DSC analysis curve proves an endothermic peak corresponds to a progressive loss of mass in TG curve which extends to 507 K and could be explained by a melting accompanied by a progressive degradation of the compound at 635 K.

Above this temperature an endothermic peak found by DSC accompanied with a major loss weight observed in TG (experimental 20%, calculated 20.5 %) indicating the decomposition of the material and the pyrolysis of the organic molecule giving a gaseous liberate with the release of chlorine molecules.

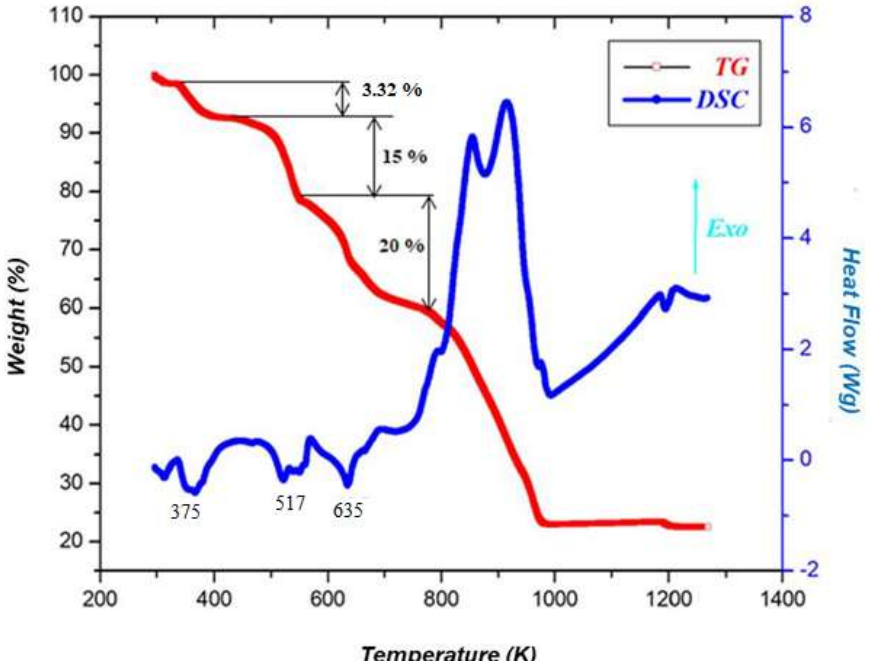

Figure 11. Simultaneous thermogravimetric and differential thermal analysis for $(C_6H_{10}N_2)[CoCl_4].H_2O$.

2.6. AIM approach

AIM (Atoms in Molecules) survey has been finished for $(C_6H_{10}N_2)[CoCl_4].H_2O$ in order to understand the existence and the steadiness of critical point indicated by BCP and numerous types of inter and intra-atomic contact bonds [30, 37-40].Fig. 12 illustrates AIM graphical analysis of using Multiwfn software at LANL2DZ level, whereas Table 6 tabulates the computational topological parameters of the title compound. When the compound is optimized with the LanL2dz basis set H ··Cl and O ··H interactions are observed. However, with the 6-31+G* basis set are predicted for the compound the N(O)-H···Cl contacts but not the H···Cl interaction. The electron density $\rho(r)$, the Laplacien $\nabla^2\rho(r)$, the eigen values of the Hessian matrix ($\lambda1$, $\lambda2$, $\lambda3$), the $\lambda1/\lambda3$ ratio, the kinetic energy densities G(r), the total energy densities H(r), the potential V(r) and the bond energy E represents the topological parameters calculated to evaluate RCP's and BCP's properties of the title crystal.

The classification of hydrogen bondscan be grouped into 3 categories:

Strong hydrogen bonds when ($\nabla^2\rho(r)$) <0 and (H(r)) < 0.

Moderate hydrogen bonds when ($\nabla^2\rho(r)$) > 0 and H(r) < 0.

Weak hydrogen bonds when ($\nabla^2\rho(r)$) > 0 and H(r) > 0.

As shown in Table 6, the AIM analysis of $(C_6H_{10}N_2)[CoCl_4].H_2O$ compound is characterized by five hydrogen bonds and that H ··Cl and O ··H interactions exhibit Cl_5 ··H_9, Cl_2 ··H_{11}, Cl_2 ··H_{24}, Cl_3 ··H_{26} and O_{24} ··N_{10} interactions.TheLaplacien of the total electron density $\nabla^2\rho$ (r_{BCP}) has been between 0.01305 and 0.05469 greater than the sum of the van der Waals.As a consequence, we can appreciate the existence of weak hydrogen bonds.In this study, from topological parameters presented in Table 6, we can perceive that $(C_6H_{10}N_2)[CoCl_4].H_2O$ is steadied by five weak Hydrogen bonds since the Laplacien and H(r) values are positive with bond energies ranging from -11.70 $kJ.mol^{-1}$ to -3.20 $kJ.mol^{-1}$. In this case, these latest results prove the presence of hydrogen bonds correspond to N(O)-H···Cl contacts observed by XRD and HS.

Table 6. Topological parameters for Hydrogen bond interactions of $(C_6H_{10}N_2)[CoCl_4].H_2O$.

Bond critical points	Density of all electrons	Laplacian of electron density	Potential energy density V(r)	Energy density E(r) or H(r)	Interaction energy (E_{int}) kJ.mol^{-1}	Electron localization function (ELF)	Localized orbital locator (LOL)	Ellipticity	Eta index
Cl_5...H_9	0.00752	0.02287	-0.00322	0.00124	-4.23	0.03308	0.15637	0.03984	0.16817
Cl_2...H_{11}	0.00804	0.05469	-0.00891	0.00237	-11.70	0.06389	0.20728	0.04146	0.18966
Cl_2...H_{24}	0.01220	0.04148	-0.00688	0.00174	-9.03	0.04417	0.17711	0.07286	0.17667
Cl_3...H_{26}	0.01361	0.04727	-0.00247	0.00077	-3.24	0.04936	0.10493	-1.29637	0.21648
O_{24}...N_{10}	0.00397	0.01305	-0.00244	0.00051	-3.20	0.01063	0.09421	1.37615	0.13664

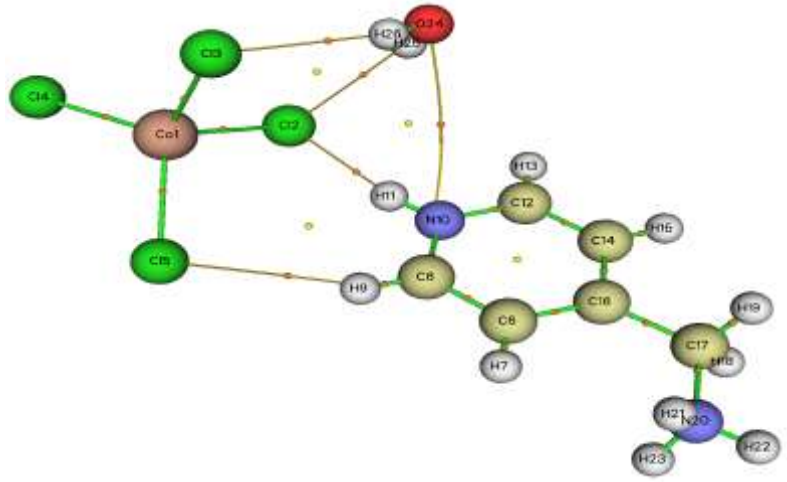

Figure 12. AIM graph of $(C_6H_{10}N_2)[CoCl_4].H_2O$ with different type of interactions.

2.10. Reduced Density Gradient (RDG) analysis

For the investigation of the type of interactions especially weak interactions like hydrogen bond, van der Waals interaction and steric effect present in hybrid material, RDG approach, improved by Johnson [41] and Contreras-Garcia et al. [42], has been developed.By using VMD and Multiwfnsoftwares, the different types of interactions of $(C_6H_{10}N_2)[CoCl_4].H_2O$ compound were visualized in Fig. 12a.The evolution of RDG (a.u) against sign $(\lambda 2)\rho$ the title crystal has been collected in Fig. 12b. We can note that λ_2 is the greatest eigenvalue of the Hessian matrix, indicates the variations of the stability of inter and intra interactions. The RDG approach has been evaluated by the following equation:

$$RDG(r) = \frac{1}{2(3\pi^2)^{1/3}} \frac{|\nabla \rho(r)|}{\rho(r)^{4/3}}$$

We can notice that the RDG peaks around −0.05, −0.02 u.a with sign $(\lambda 2)\rho$ correspond to a strong attractive interaction NCI confirmed also by AIM analysis. The intensity and types of bonds can be easily identified from the different color coded. As shown in Fig. 12b, The red color spots represents to repulsive interactions (steric effect) mainly characterized by sign $(\lambda 2)\rho > 0$. The blue color regions performed for the attractive interactions (hydrogen bonds) by sign $(\lambda 2)\rho < 0$ **[43]**. The region circled in green depicts the van der Waals interactions (weak interaction) and possessed a sign $(\lambda 2)\rho$ nearly to zero.As evidently seen, these interactions are established on the properties of electron density. The light blue spot between the chlorine atom and the hydrogen atom indicate the creation of a

Strong attractive contact N-H ··Cl and O-H ··Cl. Furthermore the green plates situated among the hydrogen atoms are ascribed to van der Waals interactions and the elliptic red plate positioned at the center of the ring and between cobalt and chlorine atoms are associated to repulsive interactions. These consequences are steady with those achieved by AIM examination and observed in the literature [14,25,44].

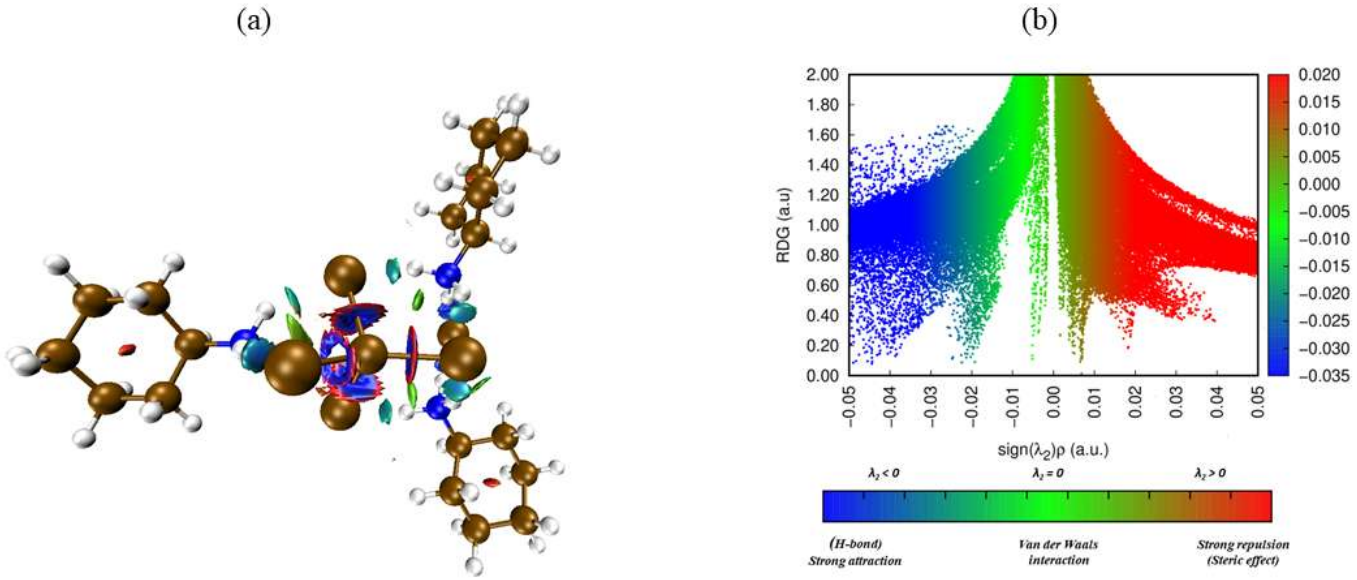

Figure 13. Visualization of different interactions using Multiwfn and VMD softwares (a), Variation of RDG as a function of ϱ multiplied by the sign of λ_2 (b) of $(C_6H_{10}N_2)[CoCl_4].H_2O$.

2.11.MEP surface analysis

MEP (Molecular Electrostatic Potential) surface allowed us to assess the locations of both electrophilic and nucleophilic attacks, as well as hydrogen bonding interactions **[24,45-46]**. The expression V(r) located at a given point r in all sides of the molecule, depends on the energy interaction between the electrons of the molecule and a proton with positive charge located in r position.MEP was optimized using DFT-theoretical method, with B3LYP/6-31G(d,p) basis set and mapped in Fig. 14. The electrostatic potential variety is defined by different colors.In the present study, the reactive sites of the nucleophilic region (positive electrostatic potential) performed by the blue color are detected around the 4AMP group, then the majority of the electrophilic sites (negative electrostatic potential) appeared with the red color are observed all over the $[CoCl_4]^{2-}$ anion, while the green or yellow color indicates the neutral region. These confirm the existence of intermolecular N–H···Cl, O-H···Cland N-H ··O interactions between the organic and the inorganic entities in the title compound.It is clearly seen that these results can prove the information concerning the region of intramolecular interaction of the title crystal.

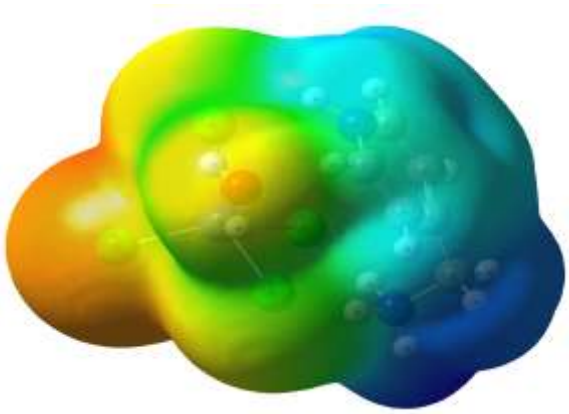

Figure 14. MEPS graphof $(C_6H_{10}N_2)[CoCl_4].H_2O$.

2.12. HOMO and LUMO analysis

To investigate the stability and the reactivity of a title compound, a computational calculation was performed using Time-Dependent DFT approach at the B3LYP/6-311++G(d,p) level to establish the frontier molecular orbital (FMO) analyzes.Fig. 15 illustrated the HOMO (highest occupied molecular orbital) and LUMO (lowest unoccupied molecular orbital) of $(C_6H_{10}N_2)[CoCl_4].H_2O$compound. It has to be noted that the positive phase is signed by red color, thought the negative phase indicated by the green color. HOMOs and LUMOs are localized on the chloride ion and the 4AMP group, respectively. Table 7 illustrated different energy parameters such as the difference of energies between HOMO-LUMO, chemical potential (μ), Electronegativity (χ), Global hardness (η), Softness (ς) and Electrophilicity(ω) which calculated via E_{HOMO} and E_{LUMO}. The orbital energy level analysis proves the E_{HOMO} and E_{LUMO} values of -6.14176 eV and -3.78406 eV, respectively. The gap energy value $\Delta E_{HOMO/LUMO}$ = 2.35 eV, reveals that $(C_6H_{10}N_2)[CoCl_4].H_2O$ has semiconductor behavior, which agrees very well to the other organic chlorocobaltate(II) compound [14]. Moreover, by demonstrating below that this compound possessed a gap energy ΔE value represents a high efficient electrical activity and a low reactivity criterion, while the higher chemical hardness (η = 1.17885) and lower chemical softness (ς = 0.42414) value indicates the stability of the molecules in the title crystal.

Table 7. Calculated energy values of $(C_6H_{10}N_2)[CoCl_4].H_2O$ compound. All values are in eV whereas ς is given in eV^{-1}.

Parameters (eV)	
E_{HOMO}	-6.14176
E_{LUMO}	-3.78406
$\Delta E = E_{LUMO} - E_{HOMO}$	**2.3577**
Chemical potential (μ)	-4.96291
Softness (ς)	0.42414
Ionization energy (I)	6.14176
Electron affinity (A)	3.78406
Electronegativity (χ)	4.96291
Chemical hardness (η)	1.17885
Electrophilicity index (ω)	10.44682

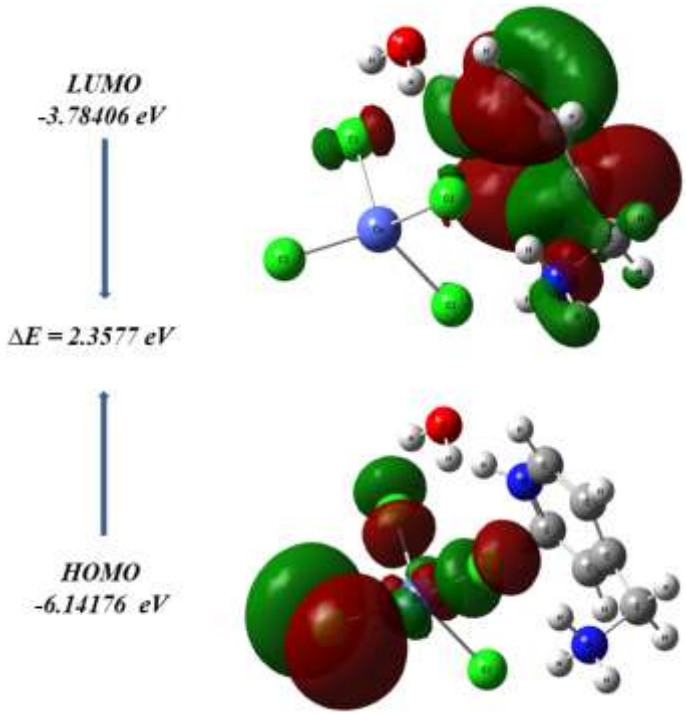

Figure 15. HOMO-LUMO plotof $(C_6H_{10}N_2)[CoCl_4].H_2O$ compound.

3.0 Materials and Methods

3.1. Materials

All products used for the synthesis of our compound: The cobalt(II) chloride hexahydrate (purity 97%), hydrochloric acid HCl (37%), 4-(aminomethyl)pyridine (purity 96%), were purchased from Sigma-Aldrich company. They are all analytical grade purity.

3.2. Synthesis and X-ray data collection

The single crystals suitable for diffraction were obtained by the slow evaporation of a solution of the compound 4AMP (1mmol) diluted in 20 mL of ethanol in a mixture of $CoCl_2{\cdot}6H_2O$ (1 mmol) and of HCl (5M), mixed for 2h under magnetic stirring at room temperature. The appeared blue crystals with prismatic shaped were collected carefully. The yield of the isolated product was 70.0%. Elemental analysis, Calc.: C, 21.89 %; H, 3.04 %; N, 8.51 %. Found: C, 21.82%; H, 3.09 %; N, 8.48 %. Elemental analyses were measured on a TruSpec Macro CHN-S analyzer. The blue crystals were collected to the X-ray data at 150 K. Bruker-AXS APEXII area detector diffractometer was used for the measurement of data employing monochromated MoKα radiation (λ = 0.71073 Å). Absorption corrections were carried out using multi-scan technique with the SADABS program **[47]**. The crystal structure was solved by SHELXT-97 software **[48]** and structural refined by SHELXL **[49]** through the WINGX program [**50**]. DIAMOND for Windows was used to preparation the figures of the structure. PXRD pattern was recorded employing D8 ADVANCE (Bruker AXS) diffractometer equipped with a Johansson Ge(111) primary monochromator giving a monochromatic Mo radiation (λ = 0.7093 Å) and using the energy-dispersive linear detector LYNXEYE XE 500 µm. Data was collected in the angular region of 2.5–45° (2θ). To acquire the compound SEM, JEOL JSM-6490 electron microscope operating at 20 kV has been applied.

3.3. Physical measurements

Infrared spectrum was recorded at room temperature between 4000–400 cm^{-1} with a Perkin-Elmer FT-IR 1000 spectrometer involving KBr and pressed into pellets. UV-Vis spectrum was carried out via a PerkinElmer Lambda

spectrophotometer. The Thermal analysis was realized employing a multimodule 92 Setaram and SDT Q600 analyzer. The sample of 11.2 mg was heated from room temperature to 1300 K at a heating speed of 5 K.min^{-1}.

3.4. Computational methodology

The experimental CIF file was used as initial theoretical structure of compound. Then, the cation structure was obtained removing the anion of structure of compound and, in the same way, the anion structure was obtained when the cation is removed. Thus, the optimizations of cation, anion and compound in gas phase were performed with the B3LYP/6-311++G** method. Hence, the natures of the reached stationary points were checked by calculating the vibrational wavenumbers. Obviously, positives frequencies were obtained for the three species indicating that these structures correspond to minimum global and they correspond to the most stable ones which were used to perform the corresponding vibrational analyses. The complete vibrational assignments of those three species were performed by using the scaled quantum mechanical force field (SQMFF) [15-17]. NBO, AIM and molecular electrostatic potential calculations at the same level of theory were predicted to investigate different intramolecular interactions and sites of reaction. To predict the reactivity of molecules, frontier molecular orbital HOMO-LUMO theory is employed while Time-dependent DFT calculations (TD-DFT) at the 6-311++G** levels of theory were applied to predict the ultraviolet-visible spectrum of compound in water using with the Gaussian program [51]. Quantum chemical calculations and molecular geometries optimizations has been achieved by the software Gaussian 09 [51] and the calculation results has been visualized with the GaussView program **[**52]. The topological investigation of non-covalent interaction was envisaged via employing Multiwfn program [53]. The softwares used for the RDG (reduced density gradient) were Multiwfn and VMD [54]. To investigate the intermolecular interactions, Hirshfeld surfaces and their associated 2D and three-dimensional (3D) fingerprints we manipulate the CrystalExplorer 3.1 program [55] via a CIF file.In addition, thermal survey (DSC-TG) have been undertaken and discussed.

4. Conclusions

In this research, we have introduced various successful tools toward a new hybrid material based on self-assembly cobalt complex template pyridine derivative. The synthesis of non-centrosymmetric organic inorganic compound $(C_6H_{10}N_2)[CoCl_4].H_2O$ at room temperature by the slow evaporation predicted, has been studied among XRD analysis. This latest revealed that the title crystal crystallized in a monoclinic system with $P2_1$ space group. The structure cohesion and stabilization have been ensured via hydrogen bonds N-H···O, N-H···Cl, O-H···Cl and C-H···Cl, thus forming a 3D-network as explored by HS and topological analysis. PXRD was proportionally agreed with the single crystal. HOMO-LUMO energies already confirmed by UV-Vis indicates that the investigated crystal have high chemical stability and low reactivity. Thermal analysis was intended to study the thermal behavior. Additionally, the MEP map defines the nucleophilic and electrophilic sites as well as the hydrogen bonding interactions. This study shows clearly that the **B3LYP/6-311++G**** DFT calculations are in good compatibility with experimental results while complete assignments were performed for the compound and its cation and anion by using the SQMFF methodology. The scaled force constants support the formation of only N-H···O and N-H···Cl interactions. Clearly, the effects of incorporation of anion in the compound are the decreasing in the scaled force constants values of cation and the slight increase in the constants corresponding to anion.

Acknowledgments: Researchers Supporting Project number (RSP2023R61), King Saud University, Riyadh, Saudi Arabia and with grants from CIUNT Project N° 26/D714 (Consejo de Investigaciones, Universidad Nacional de Tucumán). The authors thank Prof. Tom Sundius for permission to use the MOLVIB program.This study was carried out within the state assignment no. 0287-2021-0012 for the Institute of Chemistry and Chemical Technology, Siberian Branch of the Russian Academy of Sciences.

Appendix

CCDC 2183425 contain the supplementary crystallographic data for this compound, and can be obtained free charge from the Cambridge Crystallographic Data Centre via www.ccdc.cam.ac.uk/data_request/cif.

References

1. A. R., Katritzky, C. W. Rees, E. F. V. Scriven. Comprehensive Heterocyclic Chemistry II. Oxford: Pergamon Press (1996).
2. S. Aayisha, T.S. Renuga Devi, S. Janani, S. Muthu, M. Raja, S. Sevvanthi. DFT, molecular docking and experimental FT-IR, FT-Raman, NMR inquisitions on "4-chloro-N-(4,5-dihydro-1H-imidazol-2-yl)-6-methoxy-2-methylpyrimidin-5-amine": Alpha-2-imidazoline receptor agonist antihypertensive agent. J. Mol. Struct., 1186 (2019) 468-481
3. A. F. Pozharski, A. T. Soldatenkov, A. R. Katritzky. Heterocycles in Life and Society. New York: Wiley. Scheiner, S. (1997).
4. O. Noureddine, N. Issaoui, M. Medimagh, O. Al-Dossary, H. Marouani, Quantum chemical studies on molecular structure, AIM, ELF, RDG and anti- viral activities of hybrid hydroxychloroquine in the treatment of COVID-19: molecular docking and DFT calculations, JKSUS, 33(2021) 101334.
5. I. B. Sivaev, Nitrogen heterocyclic salts of polyhedral borane anions: from ionic liquids to energetic materials Chem. Heterocycl. Compd, 53 (2017) 638–658.
6. C. Ben Mleh, S. A. Brandán, N. Issaoui, T. Roisnel, H. Marouani, Synthesis, molecular structure, vibrational and theoretical studies of a new non-centrosymmetric organic sulphate with promising NLO properties, J. Mol. Struct., 1171 (2018) 771–785
7. H. L. Kwong, H. L. Yeung, C. T. Yeung, W. S. Lee, C. S. Lee, W. L. Wong, Chiral pyridine-containing ligands in asymmetric catalysis, Coord. Chem. Rev., 251 (2007) 2188.
8. D. Sinha, A. K. Tiwari, S. Singh, G. Shukla, P. Mishra, H. Chandra, A. K. Mishra,Synthesis, characterization and biological activity of Schiff base analogues of indole-3-carboxaldehyde, Eur. J. Med. Chem., 43 (2008) 160.
9. S. Bawa, S. Kumar, J. Indian. Chem., B 48 (2009) 142.
10. A. Jarrahpour, D. Khalili, C. E. De, C. Salmi, J. M. Brunel, J. Michel, Synthesis, Antibacterial, Antifungal and Antiviral Activity Evaluation of Some New bis-Schiff Bases of Isatin and Their Derivatives, Molecules 12 (2007) 1720.
11. F. Garci, H. Chebbi, N. Rouzbehd, L. Rochelsd, S. Dischd, A. Klein, M. F. Zid, Structure, Optical and Magnetic Properties of 707 the PyridiniumCobaltate ($(C_6H_9N_2)_2[CoCl_4]$, SSRN (2022) 41. 708
12. M. Khalfa, A. Oueslati, K. Khirouni, M. Gargouri, A. Rousseau, J. Lhoste, J.-F. Bardeau, G. Corbel, Synthesis, structural and 709 electrical characterization of a new organic inorganic bromide: $[(C_3H_7)_4N]_2CoBr_4$, RSC Adv., 12 (2022) 2798-2809.
13. M. Tahenti, S. Gatfaoui, N. Issaoui, T. Roisnel, H. Marouani, A tetrachlorocobaltate(II) salt with 2-amino-5-picolinium: synthesis, theoretical and experimental characterization, J. Mol. Struct., 1207 (2020) 127781.
14. M. Tahenti, N. Issaoui, T. Roisnel, H. Marouani, O. Al-Dossary, A. S. Kazachenko, Self-assembly of a new cobalt complex, $(C_6H_{14}N_2)_3[CoCl_4]Cl$: Synthesis, empirical and DFT calculations, J. King. Saud. University., 34 (2022) 101807.
15. P. Pulay, G. Fogarasi, G. Pongor, J.E. Boggs, A. Vargha, J. Am. Chem. Soc., 105 (1983) 7073.
16. G. Rauhut, P. Pulay, Transferable Scaling Factors for Density Functional Derived Vibrational Force Fields. J. Phys. Chem. 99 (1995) 3093-3100.
17. T. Sundius, Scaling of ab-initio force fields by MOLVIB. Vib.Spectrosc. 29 (2002) 89-95.
18. H. Marouani, M. Rzaigui, S. S. AL-Deyab, Synthesis and Crystal Structure of $(3\text{-}NH_3CH_2C_5H_4NH)SO_4{\cdot}H_2O$, X-ray Structure Analysis (2011), VOL. 27.
19. B. F. Ali, R. Al-Far, S. F Haddad, 3-(Ammoniomethyl)pyridiniumdibromide, Acta Cryst. (2012). E68, o3066.
20. M. Landolsi, S. Abid, Crystal structure and Hirshfeld surface analysis of trans-2,5-dimethylpiperazine-1,4-diium tetrachloridocobaltate(II), ActaCrystallogr., E77 (2021) 424–427.
21. A. R. Song, I. C. Hwang, K. Ha, Crystal structure of bis(2- (amminiomethyl)pyridinium) hexachloromanganate(II) dehydrate, $(C_6H_{10}N_2)_2[MnCl_6].2H_2O$, Z. Kristallogr. NCS 222 (2007) 43-44.
22. M. Schutte, H. G. Visser, A. Roodt, 2-(Ammoniomethyl)pyridinium sulfate monohydrate, ActaCryst. (2012). E68, o914.
23. I. D, Brown. ActaCrystallogr., A32 (1976) 24.
24. S. Trabelsi, N. Issaoui, S. A. Brandán, F.Bardak, T. Roisnel, A. Atac, H. Marouani, Synthesis and physic-chemical properties of a novel chromate compound with potential biological applications, bis(2-phenylethylammonium) chromate(VI), J Mol. Struct. 1185 (2019) 168-182
25. M. Tahenti, N. Issaoui, T. Roisnel, H. Marouani, Synthesis, characterization, and computational survey of a novel material template o-xylylenediamine, J. Iran. Chem. Soc., 19 (2022)1499–1514.
26. I.Chaabane, F.Hlel, K. Guidara, Synthesis, Infra-red, Raman, NMR and structural characterization by X-ray Diffraction of $(C_{12}H_{17}N_2)_2CdCl_4$ and $(C_6H_{10}N_2)_2Cd_3Cl_{10}$ compounds. PMC Physics B, 1 (2008) 11.
27. T.K. Kuruvilla, S. Muthu, J. C. Prasana, J. George, S. Sevvanthi. Spectroscopic (FT-IR, FT-Raman), quantum mechanical and docking studies on methyl[(3S)-3-(naphthalen-1-yloxy)-3-(thiophen-2-yl)propyl]amine. J. Mol. Struct. 1175, 2019, 163-174
28. S. Muthu, E. Elamurugu Porchelvi, M. Karabacak, A.M. Asiri, Sushmita S. Swathi. Synthesis, structure, spectroscopic studies (FT-IR, FT-Raman and UV), normal coordinate, NBO and NLO analysis of salicylaldehyde *p*-chlorophenylthiosemicarbazone. J. Mol. Struct. 1081 (2015) 400-412.
29. N. Issaoui, H. Ghalla, F.Bardak, M. Karabacak, N. AouledDlala, H.T. Flakus, B. Oujia, Combined experimental and theoretical studies on the molecular structures, spectroscopy, and inhibitor activity of 3-(2-thienyl)acrylic acid through AIM, NBO,FT-IR, FT-Raman, UV and HOMO-LUMO analyses, and molecular docking, J. Mol. Struc, 1130 (2017) 659 - 668.
30. A. Sagaama, N. Issaoui, O. Al-Dossary, A.S. Kazachenko, M. J.Wojcik, Non-covalent interactions and molecular docking studies on morphine compound, J. King Saud University - Science, 33(8) (2021) 101606.

31. I. Ben Saad, N. Hannachi, T. Roisnel, F. Hlel, Ionic organic-inorganic ($C_6H_{10}N_2$) (Hg_2Cl_5)$_2$·3H_2O compound: Structural study, Hirshfeld surface, thermal behavior and spectroscopic studies, J.Mol.Struct., 1178 (2018) 201-211.
32. M.J. Márquez, D. Romani, S.B. Díaz, S.A. Brandán, Structural and vibrational characterization of anhydrous and dihydrated species of trehalose based on the FTIR and FTRaman spectra and DFT calculations, Journal of King Saud University 30 (2018) 229-249.
33. M. Ben Jomaa, H. Chebbi, H. Ferjani, S. García-Granda, N. Korbi, N. Fakhar Bourguiba, Structural and spectroscopic studies, DFT calculations, thermal characterization and antimicrobial activity of cobalt(II) organic-inorganic hybrid material with benzamidinium cation, J. Coord. Chem, 74 (9-10) (2021) 1505–1521.
34. N. Chihaouia, B. Hamdi, T. Dammak, R. Zouari, Molecular structure, experimental and theoretical spectroscopic characterization and non-linear optical properties studies of a new non-centrosymmetric hybrid material, J. Mol. Struct., 1123 (2021) 144–152.
35. B.D. Viezbicke, S. Patel, B.E. Davis, D.P. Birnie, Evaluation of the Tauc method for optical absorption edge determination: ZnO thin films as a model system, Phys. Status Solidi B, 252(8) (2015) 1700.
36. A. Abkari, I. Chaabane, K. Guidara, Synthesis, crystal structure, spectroscopic characterization and optical properties of bis(4-acetylanilinium) tetrachlorocobalt (II). Physica E: Low-Dimensional Systems and Nanostructures, 86 (2017) 210–217.
37. A. Ramalingam, S. Sivakumar, M. Medimagh, O. Al-Dossary, N. Issaoui, M. J.Wojcik, Study of a new piperidone as an anti-Alzheimer agent: Molecular docking, electronic and intermolecular interaction investigations by DFT method, J. King Saud University - Science, 33(8) (2021) 101632.
38. M. Hanif, N. Kosar, T. Mahmood, M. Muhammad, F. Ullah, M. Nawaz Tahir, A.I. Ribeiro, E. Khan. Schiff Bases Derived from 2-Amino-6-methylbenzothiazole, 2-Amino-5-chloropyridine and 4-Chlorobenzaldehyde: Structure, Computational Studies and Evaluation of Biological Activity. ChemistrySelect, 7 (2022) e202203386
39. M. Arshad, K. Ahmed, M. Bashir, N. Kosar, M. Kanwal, M. Ahmed, H.U. Khan, S. Khan, A.Rauf, A. Waseem, T. Mahmood. Synthesis, structural properties and potent bioactivities supported by molecular docking and DFT studies of new hydrazones derived from 5-chloroisatin and 2-thiophenecarboxaldehyde. J. Mol.Struct. 1246, 2021, 131204.
40. M. N. Ahmed, S. Shabbir, B. Batool, T. Mahmood, U. Rashid, K. A. Yasin, M. N. Tahir, M. L. Arias Cassará, D.M. Gil. A New Insight into Non-covalent Interactions in 1,4-Disubstituted 1*H*-1,2,3-Triazole: Synthesis, X-ray structure, DFT calculations, *in vitro* Lipoxygenase Inhibition (LOX) and *in silico* Studies. J. Mol.Struct. 1236, 2021, 130283.
41. E.R. Johnson, S. Keinan, P. Mori-Sanchez, J. Contreras-García, A.J. Cohen, W. Yang, J. Am. Chem. Soc. 132 (2010) 6498-6506.
42. J. Contreras-Garcia, W. Yang, E.R. Johnson, Analysis of hydrogen-bond interaction potentials from the electron density: integration of noncovalent interaction regions, J. Phys. Chem. A 115 (2011) 12983-12990.
43. M. Medimagh, N. Issaoui, S. Gatfaoui, O. Al-Dossary, A. S. Kazachenko H. Marouani, Molecular modeling and biological activity analysis of new organic-inorganic hybrid: 2-(3,4-dihydroxyphenyl) ethanaminium nitrate, J. King Saud University - Science, 33(8) (2021) 101616.
44. M. Jomaa, N. Issaoui, T. Roisnel, H. Marouani, Insight into non-covalent interactions in a tetrachlorocadmate salt with promising NLO properties: Experimental and computational analysis, J. Mol. Struc, 124215 (2021) 130730.
45. P. Politzer, J. Murray, Theor. Chem. Acc. 108 (2002) 134-142.
46. A. S. Kazachenko, F. Akman, A. Sagaama, N. Issaoui, Y. N. Malyar, N. Yu. Vasilieva, V. S. Borovkova, Theoretical and experimental study of guar gum sulfation, Journal of Molecular Modeling, 5 (2021).
47. Bruker , APEX2, SAINT and SADABS , Bruker AXS Inc, Madison, Wisconsin, USA, 2006.
48. G. M. Sheldrick, SHELXT – Integrated space -group and crystal structure determination .ActaCryst. A 71 (2015) 3 – 8.
49. G. M. Sheldrick, Crystal structure refinement with SHELXL, ActaCryst. C 71 (2015) 3 – 8.
50. L.J. Farrugia, WinGX and ORTEP for windows: an update, J. Appl. Cryst. 45 (2012) 849-854.
51. M.J. Frisch, et al., GAUSSIAN 09, Revision A.02, Gaussian, Inc., Wallingford CT (2009).
52. R. Dennington, et al. GaussView, Version 5 (Semichem.Inc Shawnee Mission, KS, (2009).
53. T .Lu ,F .Chen ,Multiwfn : a multifunctiona l wavefunction analyzer . J. Comput .Chem . 33 (2012) 580 –592 .
54. W. Humphrey, A. Dalke, K. Schulten, VMD: Visual molecular dynamics, J. Mol. Graph. 14 (1996) 27-38.
55. S.K. Wolff, D.J. Grimwood , J.J. McKinnon , D. Jayatilaka , M.A. Spackamn , Crystal Explorer 3.1, University of Westren Australia, Perth. 773 (2013).